

From outburst to quiescence: the decay of the transient AXP XTE J1810–197

F. Bernardini^{1,2}, G. L. Israel², S. Dall’Osso^{4,2}, L. Stella², N. Rea³, S. Zane⁶, R. Turolla^{6,7}, R. Perna⁸, M. Falanga⁹, S. Campana⁵, D. Götz⁹, S. Mereghetti¹⁰, and A. Tiengo¹⁰

¹ Università degli Studi di Roma “Tor Vergata” Via Orazio Raimondo 18, I–00173 Roma, Italy

² INAF – Osservatorio Astronomico di Roma, Via Frascati 33, I–00040 Monteporzio Catone (Roma), Italy.

³ University of Amsterdam, Astronomical Institute “Anton Pannekoek”, Kruislaan, 403, 1098 SJ, Amsterdam, The Netherlands

⁴ Dipartimento di Fisica “Enrico Fermi”, Università di Pisa, Largo B. Pontecorvo 3, I–56127 Pisa, Italy

⁵ INAF – Osservatorio Astronomico di Brera, Via Bianchi 46, I–23807 Merate (Lc), Italy

⁶ Mullard Space Science Laboratory University College of London Holmbury St Mary, Dorking, Surrey, RH5 6NT, UK

⁷ Department of Physics, University of Padova, Via Marzolo 8, I–35131 Padova, Italy

⁸ JILA, Univ. of Colorado, Boulder, CO 80309–0440, USA

⁹ CEA Saclay, DSM/DAPNIA/Service d’Astrophysique, F–91191, Gif sur Yvette, France

¹⁰ INAF – Istituto di Astrofisica Spaziale e Fisica Cosmica Milano, Via Edoardo Bassini 15, 20133 Milano, Italy

ABSTRACT

Aims. XTE J1810–197 is the first transient Anomalous X–ray Pulsar ever discovered. Its highly variable X–ray flux allowed us to study the timing and spectral emission properties of a magnetar candidate over a flux range of about two orders of magnitude.

Methods. We analyzed nine *XMM–Newton* observations of XTE J1810–197 collected over a four years baseline (September 2003 – September 2007). EPIC PN and MOS data were reduced and used for detailed timing and spectral analysis. Pulse phase spectroscopic studies were also carried out for observations with sufficiently high signal to noise.

Results. We find that: (i) a three blackbodies model reproduces the spectral properties of XTE J1810–197 over the entire outburst statistically better than the two blackbodies model previously used in the literature, (ii) the coldest blackbody is consistent with the thermal emission from the whole surface, and has temperature and radius similar to those inferred from *ROSAT* observations before the outburst onset, (iii) there is a spectral feature around 1.1 keV during six consecutive observations (since March 2005); if due to proton resonant cyclotron scattering, it would imply a magnetic field of $\sim 2 \times 10^{14}$ G. This is in a very good agreement with the value from the spin period measurements.

Key words. stars: pulsars: individual: XTE J1810–197 – stars: magnetic fields – stars: neutron – X–rays: stars

1. Introduction

Despite isolated neutron stars as a whole are relatively poor X–ray emitters, two small classes of objects stand out for their widely variable high energy emission, which covers several orders of magnitude both in intensity and in timescales. These objects are the Anomalous X–ray Pulsars (AXPs; ten objects plus one candidate) and Soft γ –ray Repeaters (SGRs; 5 objects plus 2 candidates; for a review see Woods et al. 2006). It is believed that AXPs and SGRs are linked at some level, owing to their similar timing properties (spin periods in the 2–12s range and period derivatives \dot{P} in the $10^{-13} \div 10^{-11}$ ss⁻¹ range). Both classes have been proposed to consist of neutron

stars whose emission is powered by the decay of their extremely strong internal magnetic fields ($> 10^{15}$ G; Duncan & Thompson 1992, Thompson & Duncan 1995). Different types of X–ray flux variability are displayed by AXPs. From slow and moderate flux changes (up to a factor of a few) on timescales of years (virtually all of the objects of the class), to moderate–intense outbursts (flux variations of a factor up to 10) lasting for 1–3 years (1E 2259+586, and 1E 1048.1–5973), to dramatic and intense SGR–like burst activity (fluences of $10^{36} - 10^{38}$ ergs) on sub–second timescales (4U 0142+614, XTE J1810–197, 1E 2259+586 and 1E 1048.1–5973; see for a review on the X–ray variability see Kaspi et al. 2007). The first notable recorded case of flux variability was the 2002 bursting/outbursting event detected from 1E 2259+586, in which a factor of ~ 10 persistent flux enhancement in an AXP was fol-

lowed by the onset of bursting activity during which the source emitted more than 80 short bursts (Gavriil et al. 2004, Woods et al. 2004). The timing and spectral properties of the source changed significantly and attained the pre-bursting activity values within a few days.

However, it was only in 2003 that the first transient AXP (TAXP), namely XTE J1810–197, was discovered (Ibrahim et al. 2004). This source was serendipitously detected by the *RXTE* satellite, and then localized and studied in greater detail with the *Chandra* and *XMM–Newton* observatories (Gotthelf et al. 2004, Israel et al. 2004; Rea et al. 2004; Gotthelf & Halpern 2005; 2007). It displayed a persistent flux enhancement by a factor of > 100 with respect to the quiescent luminosity level of $\sim 10^{33} \text{erg s}^{-1}$ (as observed by *ROSAT* and *Einstein* observatories). Unfortunately, the initial phases of the outburst were missed and we do not know whether a bursting phase, similar to that of 1E 2259+586, occurred also for this source soon after the onset of the outburst. However, four bursts were detected by *RXTE* between September 2003 and April 2004 and unambiguously associated with XTE J1810–197 (Woods et al. 2005). By using *Very Large Array* (VLA) archival data, Helfand et al. (2005) discovered a transient radio emission with a flux of $\sim 4.5 \pm 0.5 \text{ mJy}$ at 1.4 GHz at the *Chandra* X–ray position of XTE J1810–197. Only later, this emission was discovered to be pulsed, highly polarized and with large flux variability even on very small timescales (at variance with all known radio pulsars; Camilo et al. 2006). The VLA data were also used to infer a proper motion of $13.5 \pm 1.0 \text{ mas yr}^{-1}$, which, assuming a distance of $3.5 \pm 0.5 \text{ kpc}$, results in a transverse velocity of $212 \pm 35 \text{ km s}^{-1}$ (1σ confidence level; Helfand et al. 2007).

Deep IR observations revealed a weak, $K_s = 20.8$ mag counterpart, with characteristics similar to those of other AXPs (Israel et al. 2004). Variability in the IR counterpart of XTE J1810–197 was found (Rea et al. 2004), but it did not correlate with the X–ray emission, contrary to earlier claims (Camilo et al. 2007a; Testa et al. 2008). It is unclear at present whether the IR variability correlates with that observed in the radio pulsed emission (Camilo et al. 2006, 2007a).

TAXPs are fairly rare objects: a second TAXP was revealed in 2006 when a candidate AXP, namely CXOU J164710.2–455216, displayed a rather intense burst followed by an outburst with a maximum flux enhancement > 300 , characterized by extreme changes in both the spectral and timing properties (Muno et al. 2006a, 2006b; Israel et al. 2007a). At variance with XTE J1810–197, CXOU J164710.2–455216 did not show any radio emission so far. The third TAXP, 1E1547.0–5408, was discovered in 2007 when its X–ray flux raised by a factor of ~ 20 above the quiescent flux. As in the case of XTE J1810–197, 1E1547.0–5408 was found to be a transient radio pulsar. Unfortunately the observations missed the outburst onset (Camilo et al. 2007b; Gelfand & Gaensler 2007; Halpern et al. 2008). The three TAXPs above are characterized by a quies-

cent state, the timing and spectral properties of which are similar to those of thousands of other X–ray sources present in the *ROSAT* catalogues: no pulsations (with the exception of CXOU J164710.2–455216) and soft X–ray spectra well fitted by a blackbody (*BB*) model with a kT of about 0.1–0.2 keV; again with the exception of CXOU J164710.2–455216, which has $kT \sim 0.5 \text{ keV}$ (Muno et al. 2006b; Skinner et al. 2006). The transient nature of these three AXPs implies that a relatively large number of members of this class has not been discovered yet, and suggests that others will manifest themselves in the future through their outbursts.

After more than four years of data since the outburst onset, XTE J1810–197 provides the first opportunity to study the timing and spectral evolution of a TAXP as it returns to its quiescent state. Since the first *XMM–Newton* 2003 observations of XTE J1810–197 (Gotthelf et al. Halpern 2004), carried out approximately one year after the outburst, it was evident that the source spectrum (two blackbodies with $kT_1 = 0.29 \pm 0.03 \text{ keV}$, $R_{\text{BB1}} \sim 5.5 \text{ km}$, and $kT_2 = 0.70 \pm 0.02 \text{ keV}$, $R_{\text{BB2}} \sim 1.5 \text{ km}$; $L_X \sim 5 \times 10^{34} \text{ erg s}^{-1}$ in the 0.5–10 keV range for a distance of 3.5 kpc) was significantly different from that in quiescence recorded by *ROSAT* in 1992 (one *BB* with $kT \approx 0.18 \text{ keV}$ and $R_{\text{BB}} \approx 10 \text{ km}$; extrapolated luminosity in the 0.5–10 keV range of $L_X \sim 7 \times 10^{32} \text{ erg s}^{-1}$; Gotthelf et al. 2004). Moreover, the source showed 5.54 s pulsations with a pulsed fraction of about 45% during outburst, while only an upper limit $\sim 24\%$ was inferred from the *ROSAT* data (Gotthelf et al. 2004).

The above properties raise a number of important, still unanswered questions: is the soft *BB* component detected by *XMM–Newton* evolving into the quiescent *BB* component seen by *ROSAT*? What happens to the higher temperature *BB* component as the source approaches quiescence? What is the pulsed fraction level of the source in quiescence (if detectable)? Is the quiescent emission revealing the Neutron Star (NS) cooling surface? Did the outburst lead to a permanent change of the timing/spectral properties such as the pulsed fraction, the flux and temperature or size of the quiescent *BB* component of the source? What is the intensity of the magnetic field of this source?

In this paper, we present a first attempt to answer the above questions through a detailed study of the timing and spectral evolution of XTE J1810–197 during its outburst decay in 2003–2007. In §2 we report the details of the *XMM–Newton* observations and our data analysis strategy. Results are presented in §3, while their implications are discussed in §4.

2. Observations and Data analysis

XTE J1810–197 was observed with *XMM–Newton* at nine epochs, the first time for just $\sim 5 \text{ ks}$, while the remaining eight observations were deeper, from $\sim 11 \text{ ks}$ to $\sim 60 \text{ ks}$ (Table 1). The *XMM–Newton* Observatory (Jansen et al. 2001) includes three $\sim 1500 \text{ cm}^2$ X–ray

Table 1. Main observational parameters for the nine *XMM–Newton* datasets. Uncertainties at 1σ confidence level are reported. The nine PN spectra were fitted together according to the prescription discussed in the text (3.2.3); the resulting reduced χ^2 (χ_{red}^2) is 1.09 (1038 d.o.f.), for the *3BB+edge* model.

Epoch	Period	Instrum. (mode)	Exp. Time	tot ph–bck ph	τ_{max} edge	Energy edge	χ_{red}^2
	s		s			keV	
Sep 2003	5.53928(3)	EPN ^b	5199	60136 – 2903	< 0.17	1.10 (fix)	1.33
		MOS1 ^d	7700	30761 – 111	< 0.02	1.10 (fix)	
Mar 2004	5.53945(1)	MOS2 ^e	7800	26739 – 145	< 0.03	1.10 (fix)	1.15
		EPN ^c	10730	71180 – 3077	< 0.18	1.10 (fix)	
		MOS1 ^e	12000	27932 – 396	< 0.03	1.10 (fix)	
Sep 2004	5.539599(6)	MOS2 ^e	12200	28809 – 366	< 0.05	1.10 (fix)	1.22
		EPN ^c	21306	89082 – 1574	< 0.17	1.10 (fix)	
		MOS1 ^e	24000	35515 – 263	< 0.06	1.10 (fix)	
Mar 2005	5.539825(6)	MOS2	timing mode	timing mode	timing mode	timing mode	timing mode
		EPN ^c	24988	54279 – 1760	0.12 ± 0.03	1.14 ± 0.02	1.05
		MOS1 ^e	37800	26501 – 428	0.09 ± 0.04	1.10 ± 0.03	
		MOS2 ^e	37800	28004 – 330	0.10 ± 0.02	0.98 ± 0.08	
EPN ^c	19787	21876 – 1311	0.26 ± 0.04	1.07 ± 0.02			
Sep 2005	5.54004(1)	MOS1 ^e	30000	10562 – 344	0.2 ± 0.1	1.13 ± 0.03	1.05
		MOS2 ^e	18000	6645 – 146	< 0.4	1.10 (fix)	“
		EPN ^c	15506	12296 – 1197	0.17 ± 0.05	1.11 ± 0.03	“
Mar 2006	5.54022(3)	MOS1 ^e	26500	6539 – 338	0.3 ± 0.3	1.48 ± 0.06	0.95
		MOS2 ^e	28000	7119 – 328	0.2 ± 0.1	1.02 ± 0.02	“
		EPN ^c	38505	23842 – 2974	0.13 ± 0.03	1.07 ± 0.02	“
Sep 2006	5.54037(1)	MOS ^e 1	46800	8113 – 552	0.20 ± 0.05	1.02 ± 0.02	1.47
		MOS2 ^e	46500	8836 – 558	0.08 ± 0.06	0.93 ± 0.03	“
		EPN ^c	37296	21903 – 2215	0.21 ± 0.04	1.07 ± 0.02	“
Mar 2007	5.54041(1)	MOS1 ^e	63000	4410 – 1897	0.14 ± 0.04	0.93 ± 0.02	0.99
		MOS2 ^e	53000	4635 – 522	0.15 ± 0.05	1.10 ± 0.02	“
		EPN ^c	59014	34386 – 4117	0.18 ± 0.02	1.04 ± 0.06	“
Sep 2007	5.540472(7)	MOS ^e 1	67910	11038 – 752	0.17 ± 0.04	1.09 ± 0.02	1.26
		MOS2 ^e	68785	12328 – 768	0.10 ± 0.03	1.1 ± 0.1	“

telescopes with an EPIC instrument in each focus, a Reflecting Grating Spectrometer (RGS; den Herder et al. 2001) and an Optical Monitor (Mason et al. 2001). Two of the EPIC imaging spectrometers use MOS CCDs (Turner et al. 2001) and one uses a PN CCD (Strüder et al. 2001). Data have been processed with SAS version 7.1.0, using the updated calibration files (CCF) available in June 2008. Standard data screening criteria are applied in the extraction of scientific products. We have cleaned all observations from solar flares by collecting CCD light curves above 10 keV and applying an intensity threshold. We also used a time window criterion for removing solar flare intervals and checked that no significant spectral differences were present with respect to the intensity threshold method.

During the September 2003 observation, the PN camera was set in **primary small window** imaging mode with a thin filter (time resolution= 5.07×10^{-3} s), while all other observations were in a **primary large window** imaging mode with a medium filter (time resolution= 4.76×10^{-2} s). All observation set-ups for MOS1 and MOS2 cameras were the same, with a time resolution of 0.3 s: **prime partial window** imaging mode and medium filter (in September 2003 the MOS1 was set in **prime full window** imaging mode, in September 2004 the MOS2 was in **Timing uncompressed** mode and data from this were not reduced). In order to extract more than 90% of the source counts, we accumulated a one-dimensional image and fitted the 1D photon distribution with a Gaussian. Then, we extracted the source photons from a circular region of radius 55'' ($\sim 90\%$ of photons) centered at the Gaussian centroid. The background for the spectral analysis is obtained (within the same PN or MOS CCD where the source lies

from an annulus region (inner and outer radii of 65'' and 100'', respectively) centered at the best source position. In the timing analysis the background was estimated from a circular region of the same size as that of the source. All of the EPIC spectra were rebinned before fitting, in order to have at least 40 counts per bin and prevent oversampling the energy resolution by more than a factor of three. Thanks to the time and spectral resolution of the EPIC instruments¹, we could carry out timing and spectral analysis over the entire set of observations and the Pulse Phase Spectroscopy (PPS) for the observations with sufficiently high signal to noise. We report here the analyses obtained with the PN data and, for comparison, also the results from the two MOS cameras.

3. Results

3.1. Timing analysis

The source event arrival time of each observation, in the 0.5–15 keV energy range, were converted into barycentric dynamical times (BDT) by means of the SAS tool **barycen** and the ($\sim 1''$ accurate) source position provided by Helfand et al. (2007). Given the complex time evolution of the period and its derivatives as derived by radio observations (Camilo et al. 2007c), we measured only the local spin period at each single *XMM–Newton* pointing by means of a phase fitting technique (events in the 0.5–10 keV energy range were used; see e.g. Dall’Osso et al. 2003 for details on the technique). Different period measurements are independent and not phase-connected.

¹ http://xmm.esac.esa.int/external/xmm_user_support/...documentation/uhb.2.5/node28.html

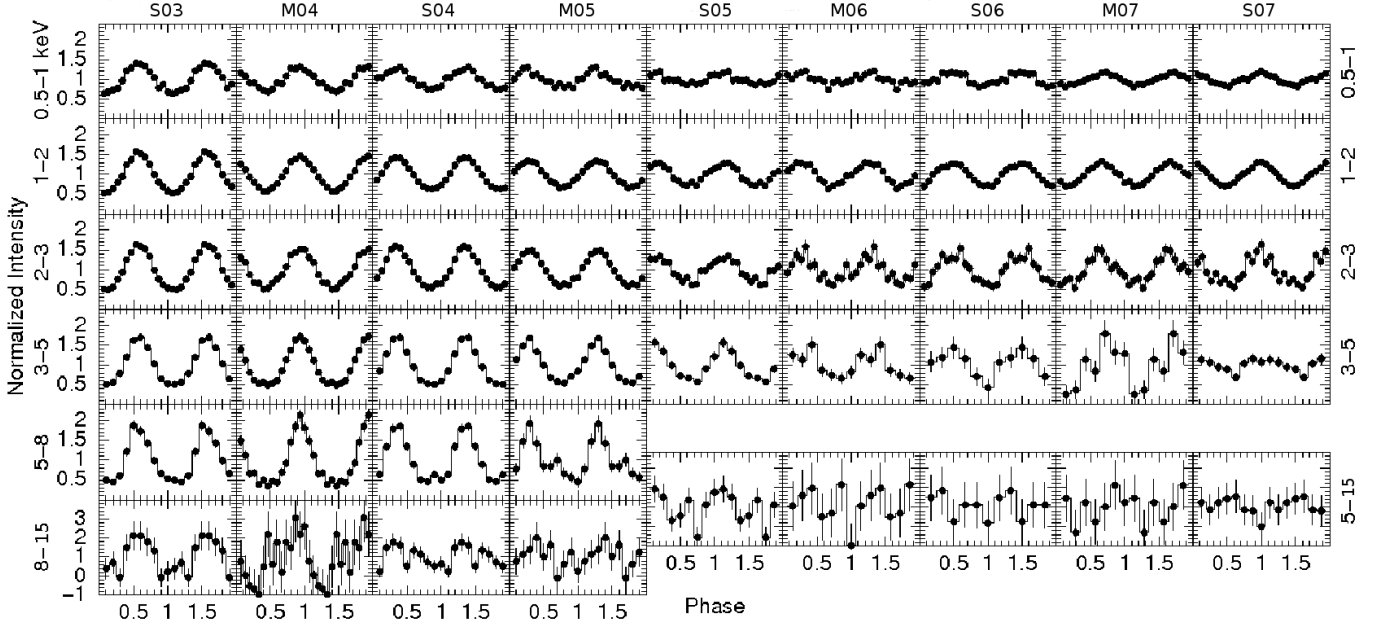


Fig. 1. XTE J1810–197 PN background subtracted light curves folded at the best period (see Table 1) for each of the nine *XMM–Newton* observations carried out between September 2003 (S03) and September 2007 (S07), and for different energy intervals: 0.5–1 keV, 1–2 keV, 2–3 keV, 3–5 keV, 5–8 keV, and 8–15 keV. The last two energy intervals have been merged together since the September 2005 (S05) pointing in order to improve the statistics.

Folding each lightcurve at its measured spin period we obtained the pulse profile and found that it remained single peaked in all observations (Figure 1). In order to estimate the dipole field strength of this source we refer to the phase-coherent measurements of ν , $\dot{\nu}$, and $\ddot{\nu}$ obtained by Camilo et al. (2007c). These authors measured fast variations of $\dot{\nu}$ that did not allow them to provide a unique value for the magnetic field strength. The frequency derivative was found to change continuously over 300 days of monitoring from $\sim -3.4 \times 10^{-13} \text{ s}^{-2}$ to $\sim -1.4 \times 10^{-13} \text{ s}^{-2}$. Accordingly, we consider the secular spindown trend as bracketed by these limits and derive a corresponding range of values for the magnetic field $1.6 \times 10^{14} \text{ G} \leq B_{\text{dip}} \leq 2.8 \times 10^{14} \text{ G}$ through the standard dipole formula.

3.1.1. Pulsed fraction

Given the smooth and nearly sinusoidal pulse shape, we could determine with reasonable accuracy the Pulsed Fraction (PF) of the signal (defined here as: $\text{PF} = (A_{\text{max}} - A_{\text{min}})/(A_{\text{max}} + A_{\text{min}})$, where A_{max} and A_{min} are the maximum and minimum of the sinusoidal modulation). Between September 2003 and September 2007, the PF decreased by a factor of about two (between $\sim 50\%$ and $\sim 25\%$) in the 0.5–10 keV energy interval (Figure 2). In particular, since March 2005, the PF in the 0.1–2.5 keV band reached $\sim (25 \pm 1)\%$ (here and throughout this paper uncertainties are given at 1σ confidence level, where not stated otherwise); this value

is close to the upper limit ($\sim 24\%$) inferred from the 1992–1993 *ROSAT* pointings during the quiescent phase of the source (Gotthelf et al. 2004).

Moreover, the PF decreases as a function of time in the same energy band and increases as a function of energy within the same observation, as shown in Table 2. Between 8 and 15 keV the pulsed fraction is consistent with 100% (3σ confidence level). However, the relatively poor statistics above 10 keV prevented a detailed study of the spectral properties of this high energy component (see also Section 3.2).

3.2. Spectral analysis

In the following we describe a detailed spectral analysis of our *XMM–Newton* dataset which includes the outburst evolution down to its almost complete decay. The outburst spectrum in its brightest phase had already been analyzed in the literature with a two blackbodies spectral model (*2BB*, Gotthelf et al. 2004, Gotthelf & Halpern 2005). On the other hand the quiescent emission from the source recorded by *ROSAT* was consistent with a different, single *BB*. Starting from this, our strategy was then twofold: first we tried to apply the *2BB* model to the whole *XMM–Newton* dataset to check whether one of the two components evolved smoothly to the quiescent one. Then we tested an alternative possibility, namely that the quiescent component was independent and always present, the spectrum of the outburst being superimposed

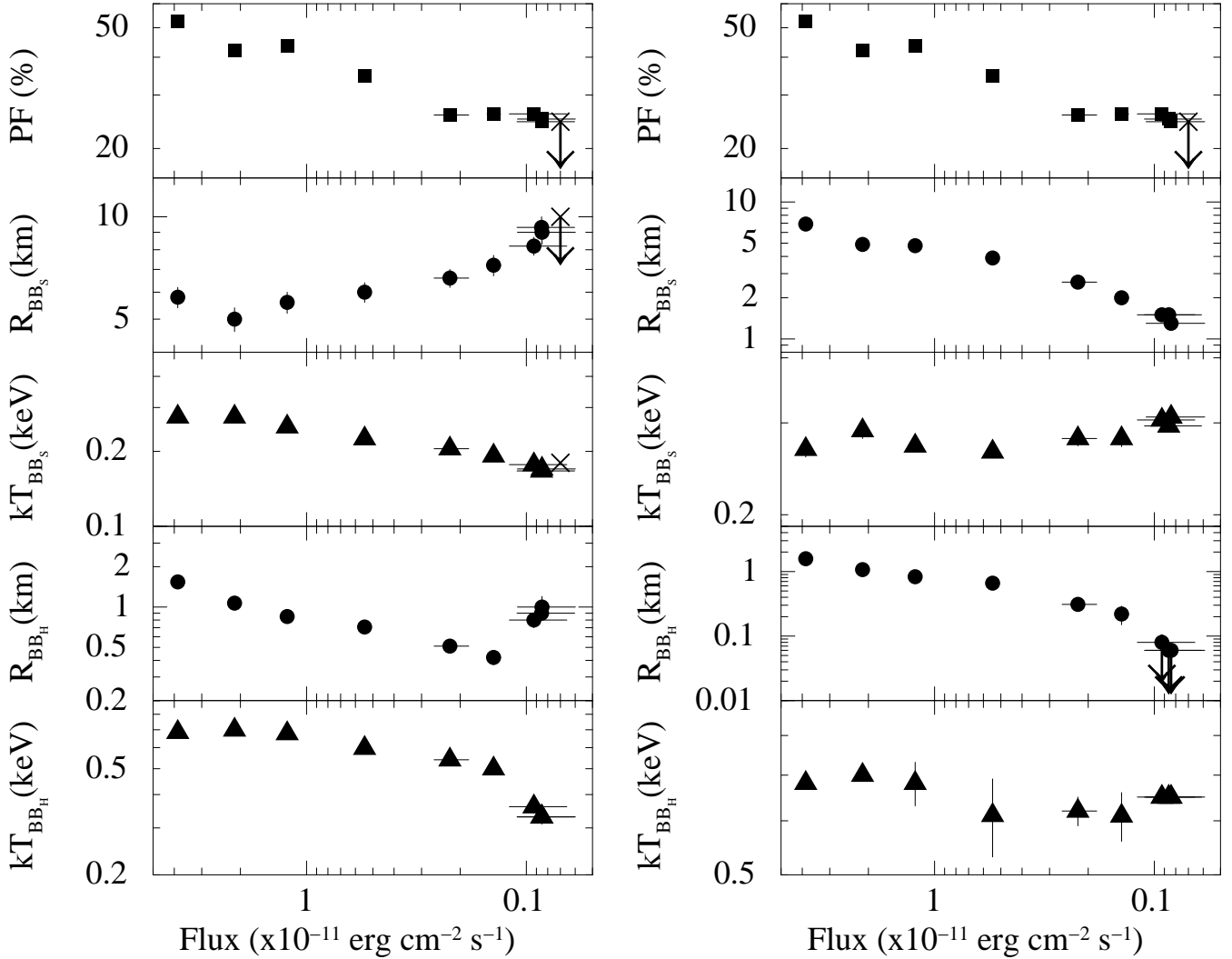


Fig. 2. Evolution of the spectral parameters for the *2BB* (left panel) and *3BB* (right panel) models together with the pulsed fraction (PF) as a function of the 0.6–10 keV flux. The cross in the left panel (first, second, and third row), and in the right panel (first row) marks the *ROSAT* data.

Table 2. Pulsed fraction (PF) in different energy intervals vs time, and $\text{PF}_{0.5\div 15}^{\text{total}}$ keV. Errors are reported at 1σ confidence level.

Epoch	$\text{PF}_{0.5\div 1 \text{ keV}}$ %	$\text{PF}_{1\div 2 \text{ keV}}$ %	$\text{PF}_{2\div 3 \text{ keV}}$ %	$\text{PF}_{3\div 5 \text{ keV}}$ %	$\text{PF}_{5\div 8 \text{ keV}}$ %	$\text{PF}_{8\div 15 \text{ keV}}$ %	$\text{PF}_{0.5\div 15 \text{ keV}}^{\text{total}}$ %
Sep 2003	35 ± 2	49.3 ± 0.5	57.0 ± 0.8	58.7 ± 0.9	63 ± 3	100 ± 20	52.4 ± 0.4
Mar 2004	25 ± 1	37.2 ± 0.5	42.1 ± 0.8	51 ± 1	66 ± 3	50 ± 25	42.0 ± 0.4
Sep 2004	27 ± 1	40.2 ± 0.7	49.6 ± 0.7	57.6 ± 0.9	63 ± 2	50 ± 12	43.5 ± 0.3
Mar 2005	20 ± 1	33.1 ± 0.6	44 ± 1	51 ± 1	49 ± 5	100 ± 40	34.8 ± 0.4
Sep 2005	13 ± 2	27.2 ± 0.9	32 ± 2	30.0 ± 0.9	60 ± 11	60 ± 30	25.8 ± 0.7
Mar 2006	13 ± 2	30 ± 1	32 ± 3	26 ± 6	70 ± 29	20 ± 48	26 ± 1
Sep 2006	16 ± 1	29.3 ± 0.9	42 ± 3	90 ± 72	90 ± 72	40 ± 41	26 ± 0.7
Mar 2007	15 ± 2	32 ± 1	36 ± 3	60 ± 10	30 ± 33	40 ± 10	25 ± 1
Sep 2007	15 ± 1	28.1 ± 0.7	41 ± 3	50 ± 10	40 ± 50	80 ± 25	24.5 ± 0.6

on it; this led us to consider a phenomenological model including three different thermal components (*3BB* model). In this scenario, as the outburst flux decays its spectral components progressively fade away eventually revealing the underlying quiescent emission. As such, the

quiescent component could be tentatively identified with the thermal emission from the whole NS surface.

3.2.1. Thermal components

Following Gotthelf et al. (2004) and Gotthelf & Halpern (2005), we applied the *2BB* spectral fit to the fading phases of XTE J1810–197 until September 2007, when the source flux was ~ 1.2 times higher than the pre–outburst level ($\chi_{red}^2 \sim 1.26$ for 1058 d.o.f., which is at $6\sigma_{\chi^2}$ from the expectation value²; $N_H = (0.60 \pm 0.01) \times 10^{22} \text{ cm}^{-2}$; see also Table 3). The *2BB* model (see also Perna & Gotthelf 2008 for a detailed study) corresponds to a scenario in which one of the two *BB* naturally evolves into the single *BB* spectrum detected by *ROSAT* in the quiescent state while the other (hard) *BB* just fades away. The results of this approach showed that, while the cold *BB* component smoothly approaches the quiescent one (see Figure 2, left panel, 2nd and 3rd plot), a number of ambiguities arise. The radius of the hot *BB* does not decrease monotonically with flux (time): after 2.5 years of smooth decrease it starts increasing in September 2006 (left panel, 4th plot). At the same epoch its temperature drops rapidly reaching a value comparable to that of the cold *BB* in the first part of the outburst (Figure 2, left panel, 5th plot). Moreover, neither spectral component is able to account for the flattening of the pulsed fraction at the 25% level, (Figure 2, left panel, 1st plot).

These findings suggest that the observed emission might come from a more complex structure than a simple two–component model and that we might be seeing different parts of the whole structure as the flux decreases. With this scenario in mind we repeated the spectral analysis using the *3BB* model discussed in the previous subsection.

For the first six observations (during which the total flux is significantly higher than the pre–outburst one), all parameters of the *3BB* model were left free to vary except for N_H which was constrained to be the same in all observations. We found that it is always possible to fit the first 6 data sets (September 2003–March 2006) with a *3BB* model without forcing the spectral parameters (*3BB*: $\chi_{red}^2 = 1.1$, 812 d.o.f.; *2BB*: $\chi_{red}^2 = 1.21$, 824 d.o.f., F–test probability $\simeq 10^{-11} \sim 7\sigma$). The extra *BB* has a characteristic temperature $kT \sim 0.14 \text{ keV}$ which is constant in time, but whose radius could not be well constrained ($R < 100 \text{ km}$). Under the hypothesis that the latter component originates from the whole NS surface, we can consider it constant through the whole outburst. Correspondingly, we left free to vary the temperature and radius of this additional *BB*, but forced both parameters to maintain the same value in all spectra.

We then applied the *3BB* model to all of the 9 *XMM–Newton* observations. The addition of the extra *BB* component gave a better fit as compared with the *2BB* model ($\chi^2 \sim 1250$, $\chi_{red}^2 \sim 1.18$ for 1056 d.o.f., $N_H = (0.72 \pm 0.02) \times 10^{22} \text{ cm}^{-2}$); an F–test gives a 7.3σ significance for the inclusion of the additional spectral component. Notably, the overall fit gave parameters for

² $\sigma_{\chi^2}^2 = 2dof \Rightarrow \sigma_{\chi^2} = \sqrt{2dof}$, $\frac{(\chi^2 - dof)}{\sigma_{\chi^2}} = x[\sigma_{\chi^2}]$, where x is the distance from the expectation value of χ^2 in unit of σ_{χ^2} .

the coldest *BB*, $kT_{cold} = 0.144 \pm 0.003 \text{ keV}$; $R_{cold} = 17.9 \pm 1.9 \text{ km}$, $F_X^{0.1-2.5 \text{ keV}} = (4.5 \pm 0.5) \times 10^{-13} \text{ erg cm}^{-2} \text{ s}^{-1}$ which are very close to those inferred in quiescence with *ROSAT* ($kT = 0.18 \pm 0.02 \text{ keV}$ and $R \sim 10 \text{ km}$, $F_X^{0.1-2.5} \sim 5.4 \times 10^{-13} \text{ erg cm}^{-2} \text{ s}^{-1}$). Even more interesting, the two hotter *BB* components maintained a nearly constant temperature as the source flux decayed in time (see Figure 2, right panel, 3rd and 5th plots). Their radius appears to be the only variable parameter during the decaying phase of the outburst (Figure 2, right panel, 2nd and 4th plots).

Starting from September 2006 the spectrum could be well fitted by a simple *2BB* model. The hottest component was not needed anymore and we could set a 3σ upper limit on its flux of $\sim 8.7 \times 10^{-14} \text{ erg cm}^{-2} \text{ s}^{-1}$. The above mentioned flattening of the pulsed fraction at this epoch could be accounted for quite naturally by the disappearance of this hot component (Figure 3).

Given the stability of both the flux and spectrum over the

Table 3. Temperature (keV) and radius (km) evolution with time of *BB*_{cold} and *BB*_{hot} in the *2BB* model. Uncertainties are at 1σ confidence level (68%).

Epoch	kT_{cold} keV	R_{cold} km	kT_{hot} keV	R_{hot} km
Sep 03	0.275 ± 0.009	5.8 ± 0.4	0.685 ± 0.005	1.54 ± 0.03
Mar 04	0.275 ± 0.009	5.0 ± 0.4	0.699 ± 0.009	1.07 ± 0.03
Sep 04	0.251 ± 0.005	5.6 ± 0.4	0.677 ± 0.005	0.85 ± 0.02
Mar 05	0.225 ± 0.004	6.0 ± 0.4	0.597 ± 0.006	0.71 ± 0.02
Sep 05	0.205 ± 0.004	6.6 ± 0.4	0.54 ± 0.01	0.51 ± 0.04
Mar 06	0.192 ± 0.004	7.2 ± 0.5	0.50 ± 0.02	0.42 ± 0.05
Sep 06	0.177 ± 0.004	8.2 ± 0.5	0.36 ± 0.02	0.8 ± 0.1
Mar 07	0.170 ± 0.005	9.0 ± 0.7	0.33 ± 0.02	1.0 ± 0.2
Sep 07	0.167 ± 0.004	9.3 ± 0.7	0.33 ± 0.01	0.9 ± 0.1

last three observations (less than 8% variation in flux in the 0.6 – 10 keV energy band; September 2006 – 2007), we merged the source photon lists in order to obtain a higher S/N spectrum (note that the calibration of the PN instrument has proved to be also very stable; Krisch et al. 2005). The analysis of the merged spectrum significantly improved the determination of the spectral parameters as compared to each single spectrum (see Table 4). Furthermore, the hotter *BB* component remained statistically non–significant also in the merged spectrum. We could thus obtain a more accurate (3σ) upper limit on its flux: $F_{BBhot} < 4.5 \times 10^{-14} \text{ erg cm}^{-2} \text{ s}^{-1}$ in the 0.6–10 keV energy band.

We also attempted to estimate the pulsed fraction of the quiescent emission, which we tentatively attributed to the NS surface, taking into account the last three observations only, so that the hotter *BB* was absent. We note that this is only possible in our scenario since in the *2BB* model the softer component is still evolving towards quiescence. We express the PF in the 0.1–1 keV band as: $PF_{(0.1-1 \text{ keV})} = \alpha F_{cold} + \beta F_{med}$, where $F_{cold} \sim 0.9$ and $F_{med} \sim 0.1$ represent the relative contributions of the two spectral components to the total flux in the 0.1–1 keV band. Correspondingly, α and β represent their PFs. The

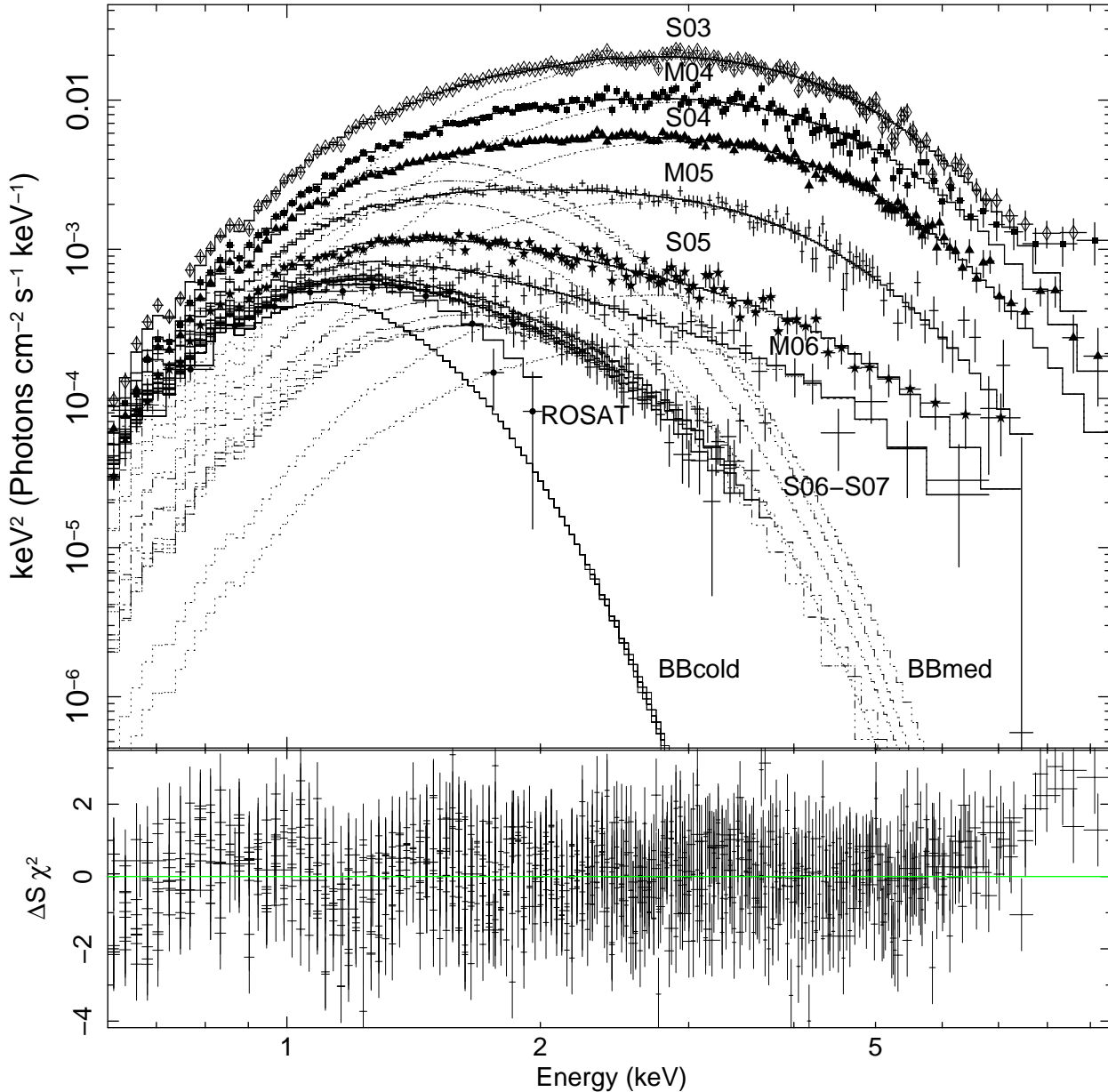


Fig. 3. Spectral evolution in the nine *XMM–Newton* observations, and the *ROSAT* spectrum in quiescence. Fits use the $3BB$ model (upper panel). Model residuals are shown in the lower panel. The soft component, constant in time, is marked with BB_{cold} ; the medium–temperature evolving blackbody component is marked with BB_{med} . There is a sharp drop in the flux above 2.5 keV in the last three spectra (compare M06 with S06, M07 and S07) which corresponds to the disappearance of the hot component BB_{hot} . M=March, S=September; 03=2003, 04=2004, 05=2005, 06=2006, and 07=2007.

value of β is obtained from the PF in the 2.8–4.1 keV energy range, where BB_{cold} is negligible, and turns out to be $\simeq 17\%$. The PF of the cold BB , α , is thus completely determined by the measured value of $\text{PF}_{(0.1-1\text{keV})}$. We obtain $\alpha = 10 \pm 1\%$, a prediction that can be checked once the source will return to the quiescent state.

3.2.2. The power–law component

By adopting the $3BB$ model, we further study the possible presence of additional features in the *XMM–Newton* spectra. In particular, during the first three *XMM–Newton* observations (2003–2004), the spectral fit residuals suggest the presence of an additional hard component above 7–8 keV (3.2σ confidence level) which we were not able to characterize due to poor statistics in this band. We can only speculate that it might be related to a hard

Table 4. Temperature, radius and observed flux (0.6–10 keV) evolution with time of *BB* medium (med) and hot *BB* (hot) in the *3BB* model. 1σ uncertainties are reported. Upper limits are inferred at 3σ confidence level.: $kT_{\text{cold}} = 0.144 \pm 0.003$ keV; $R_{\text{cold}} = 17.9 \pm_{1.5}^{1.9}$ km, $N_{\text{H}} = (0.72 \pm 0.02) \times 10^{22}$ cm $^{-2}$ are constant throughout the outburst.

Epoch	kT_{med} keV	R_{med} km	F_{med} erg s $^{-1}$ cm $^{-2}$
Sep 03	0.267 ± 0.009	6.9 ± 0.6	$(5 \pm 1) \times 10^{-12}$
Mar 04	0.29 ± 0.01	4.9 ± 0.4	$(4 \pm 1) \times 10^{-12}$
Sep 04	0.271 ± 0.006	4.8 ± 0.3	$(2.6 \pm 0.5) \times 10^{-12}$
Mar 05	0.264 ± 0.007	3.9 ± 0.3	$(1.5 \pm 0.3) \times 10^{-12}$
Sep 05	0.280 ± 0.009	2.6 ± 0.2	$(9 \pm 2) \times 10^{-13}$
Mar 06	0.28 ± 0.01	2.0 ± 0.2	$(6 \pm 2) \times 10^{-13}$
Sep 06	0.304 ± 0.006	1.5 ± 0.1	$(5 \pm 1) \times 10^{-13}$
Mar 07	0.296 ± 0.006	1.5 ± 0.2	$(4 \pm 1) \times 10^{-13}$
Sep 07	0.308 ± 0.006	1.3 ± 0.1	$(4 \pm 1) \times 10^{-13}$
Sep 06-07	0.301 ± 0.003	1.42 ± 0.03	$(4.1 \pm 0.2) \times 10^{-13}$
Epoch	kT_{hot} keV	R_{hot} km	F_{hot} erg s $^{-1}$ cm $^{-2}$
Sep 03	0.681 ± 0.005	1.58 ± 0.04	$(3.3 \pm 0.2) \times 10^{-11}$
Mar 04	0.70 ± 0.01	1.07 ± 0.04	$(1.7 \pm 0.2) \times 10^{-11}$
Sep 04	0.68 ± 0.05	0.83 ± 0.02	$(9.2 \pm 0.7) \times 10^{-12}$
Mar 05	0.61 ± 0.08	0.66 ± 0.03	$(3.5 \pm 0.5) \times 10^{-12}$
Sep 05	0.62 ± 0.03	0.31 ± 0.05	$(8 \pm 4) \times 10^{-13}$
Mar 06	0.61 ± 0.05	0.22 ± 0.07	$(4 \pm 3) \times 10^{-13}$
Sep 06	0.65^a	< 0.08	$< 8.7 \times 10^{-14}$
Mar 07	0.65^a	< 0.06	$< 6.1 \times 10^{-14}$
Sep 07	0.65^a	< 0.06	$< 5.4 \times 10^{-14}$
Sep 06-07	0.65^a	< 0.05	$< 4.5 \times 10^{-14}$

^a Fixed to the average of the earliest measurements.

power-law-like tail ($\Gamma \sim 1.5$), likely of magnetospheric origin. A similar component has been detected in other AXPs (Kuiper et al. 2004; Kuiper et al. 2006) and extends up to 200 keV, at least (Götz et al. 2006). Given the marginal significance of this component we do not attempt to draw any firm conclusion.

3.2.3. Narrow spectral feature search

Starting from the 4th observation (March 2005) we note the presence of excess residuals in the data with respect to the *3BB* model, at around 1.1 keV (Figure 4). We tried to account for this by including an absorption edge or a Gaussian line in the model. The value of the former is 1 if $E \leq E_c$ and $\exp[-\tau_{\text{max}}(E/E_c)^{-3}]$ if $E \geq E_c$ where E_c is the threshold energy and τ_{max} the absorption depth at the threshold.

The results of the new spectral model, *3BB* plus edge, are consistent with what was obtained with the *3BB* model (to within the uncertainties): $N_{\text{H}} = (0.73 \pm 0.02) \times 10^{22}$ cm $^{-2}$, $kT_{\text{cold}} = 0.153 \pm 0.005$ keV and $R_{\text{cold}} = 15.4 \pm 1.8$ km ($\chi^2 = 1140$ with d.o.f. = 1038). The energy threshold (~ 1.1 keV) and τ_{max} (~ 0.2) appear to be constant through the latest six observations (Table 1 and Figure 5).

This new model has $\chi_{\text{red}}^2 = 1.09$, which is at $2.2\sigma_{\chi^2}$ from the expectation value. To obtain an estimate of the significance of the edge component we proceeded as follows:

We obtained, for each single spectrum, the width of the

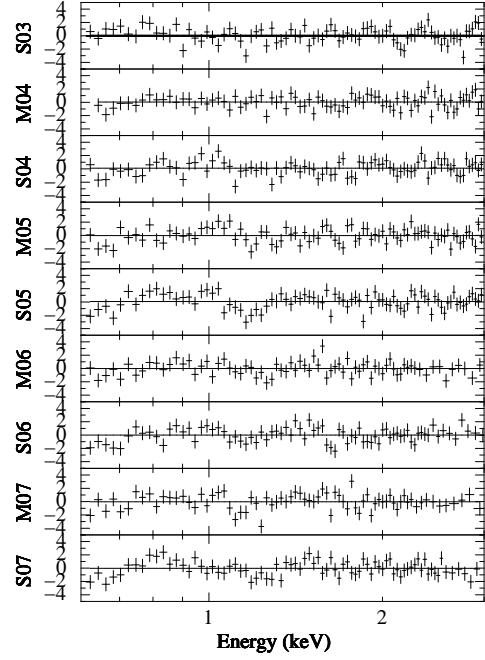


Fig. 4. $\Delta\chi^2$ residuals of *3BB* model. From March 2005 (M05) onwards is likely present a feature (edge) around ~ 1.1 keV.

feature (σ) using a Gaussian profile and defined the width at the base of the Gaussian (ΔE_i) to be 3σ . We assumed that the width of the feature is independent of the model used to estimate it. Then we calculated the ratio between the whole spectral range of our data, ΔW_i , and the Gaussian width ΔE_i (number of trials). Finally, in order to obtain the total probability of the null hypothesis (no line present), we multiplied the probability level (P_i) attributed by an F-Test to the inclusion of the Gaussian by the number of trials on each spectrum ($\Delta W_i/\Delta E_i$) and by the total number of observations (9). The total probability can thus be expressed as: $9 \times \Pi_i P_i \Delta W_i/\Delta E_i$, which gave in our case a significance for the edge component at the $\simeq 6.5\sigma$ level.

As a further check, we estimated the line significance by running a Monte Carlo simulation of 10^5 spectra with only the continuum model present (as described in more detail in Rea et al. 2005, 2007). Spectral parameters of the continuum were allowed to vary within 3 sigma from their best fit values and we used the same number of photons of the 4th observation (March 2005). We then counted how many edges, at any energy between 0.5-10keV, with $\tau > 0.2$ have been significantly detected in the generated spectra just due to statistical fluctuations. We found 12 spectra over 10^5 spectra presenting such a feature, thus leading to an estimated significance level of $\sim 4.1\sigma$ for our 1.1 keV edge. However, so far we did not consider that the feature has been detected in several spectra rather than only in the 4th observation. To this aim we simulated 10^5 spectra for each of the 6 observations showing the ~ 1.1 edge, using the best fit spectral parameters and

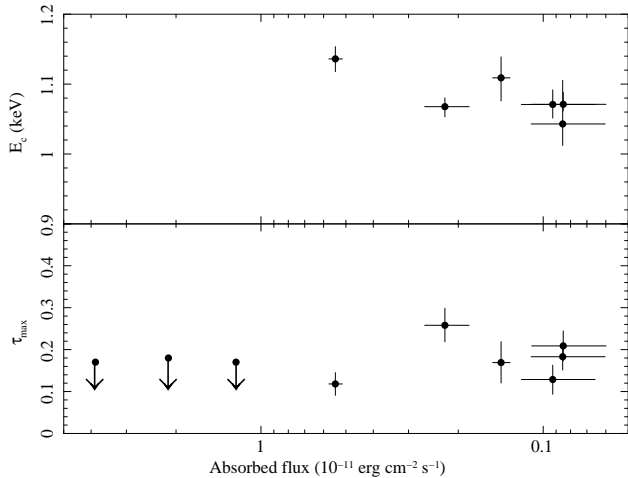


Fig. 5. Parameters of the ~ 1.1 keV edge (energy (E_c) and τ_{\max}) vs the observed flux. For the first three observations τ_{\max} is an upper limit.

the corresponding number of photons for each observation. However, in these simulations we only considered the energy band 0.5–4 keV in which the spectral variability was not so large among the 6 observations. This reduces to negligible levels any possible systematic error in the probability calculation due to the spectral variability of the source in connection with instrumental response matrices. We estimated the significance of the edge in each observation as described above, then combined them to obtain a total significance of 5.1σ for the presence of the line.

By using a Gaussian profile to fit the feature, we obtained results similar to those of the edge component, the mean energy of the feature being $\langle E \rangle \sim 1.15$ keV, $\langle \sigma \rangle \sim 0.13$ keV, while the average equivalent width of the line was ~ 35 eV ($\chi_{\text{red}}^2 = 1.09$, 1029 d.o.f.).

The use of different chemical abundances for the interstellar medium (ISM), vphabs model in *XSPEC*, does not produce significant changes in the parameter values or confidence level of the feature, which thus does not seem to depend on the ISM composition.

In order to test the possible instrumental nature of the feature we also used the source photons collected by the MOS1 and MOS2 cameras. As in the case of the PN data, we carried out a spectral analysis by using the *3BB* model to account for the continuum spectral component. Table 1 summarizes the results of this test. Starting from the March 2005 observation, the edge component is always detected in all three cameras except for the September 2005 observations MOS2 data, where only an upper limit could be obtained. In the latter case the inferred upper limit is consistent with the values inferred from all other spectra. This finding further supports the interpretation of the edge as intrinsic to the source.

To further check our results we analyzed the only *CHANDRA* public observation of XTE J1810–197 made with *ACIS*, during March 2006 (~ 30 ks). We used *CIAO* 4.0 software, a standard reduction procedure, and

the last calibration files available (3.5.0, October 2008) for the *CHANDRA* data analysis. This gives fully consistent results with those obtained with *XMM–Newton*: $E_c = 1.05 \pm 0.3$, $\tau_{\max} = 0.38 \pm 0.9$. The significance for the inclusion of this component, determined using the procedure previously exposed, is $\sim 4.5\sigma$. This provides further confirmation for the presence of this feature in the continuum of the source. Therefore in the following we consider the *3BB*+edge as our best spectral model.

3.2.4. Other models

An alternative possibility to model the data is by considering the effect of resonant Compton scattering (RCS) in the magnetosphere (Thompson, Lyutikov & Kulkarni 2002). In this scenario, photons emitted by the star surface, at the temperature of ~ 0.16 keV, are upscattered by energetic electrons and/or positrons in the magnetosphere. Therefore, the increase in X–ray flux during the outburst would not be due (only) to the appearance of (hotter) regions with enhanced emission, but to a shift in energy of upscattered photons.

We have performed some tests with a thermal Comptonization model readily available in *XSPEC* (*CompTT*, Titarchuk 1994). Although based on completely different physical assumptions with respect to RCS, this may at least be used to assess whether the observed spectra can be modelled in terms of Comptonization. We fitted together all the 9 spectra assuming, as a first approximation, that the plasma temperature is the same at all epochs. A best fit is obtained with an electron temperature of $kT_e \sim 0.8$ keV, a constant (within uncertainties) temperature for the seed photons of $kT_{\text{seed}} \sim 0.16$ keV and a plasma optical depth (τ_p) decreasing with time from ~ 32 to ~ 9 . The χ_{red}^2 , however, is worse than that of the *3BB* model, namely $\chi_{\text{red}}^2 = 1.3$ for 1066 d.o.f. (this value is at $6.7\sigma_{\chi^2}$ from the expectation value). We note also that a scenario in which scattering is (nearly) isotropic and the Comptonizing medium uniformly covers the star surface is hardly compatible with the observed characteristics of the pulsed emission. Indeed, the (relatively) small pulsed fraction of the thermal component would be further washed away by scattering at higher energies.

Also in this case a feature in the spectrum around 1.1 keV seems to be present. By fitting this feature with an edge component, like in the case of the *3BB* model, we obtain a significance level of $\sim 6.5\sigma$. Therefore, this feature seems to be independent on the model used for the underlying spectral continuum.

3.3. Pulse Phase Spectroscopy

In order to understand the role of each spectral parameter in producing the observed $0.6 \div 10$ keV flux variation with pulse phase, we carried out a pulse phase resolved spectroscopic analysis of the *XMM–Newton* observations with

sufficiently high S/N. The spectra of the first three observations (September 2003–September 2004) were considered and divided into 10 phase intervals, in order to rely upon a sufficiently large number of photons. The spectrum in each phase interval was modelled with $3BB$ s fixing the temperature and radius of BB_{cold} and N_{H} at the average values obtained from the previous analysis without the inclusion of the edge ($kT_{\text{cold}} = 0.144 \pm 0.003$ keV; $R_{\text{cold}} = 17.9 \pm 1.9$ km, $N_{\text{H}} = (0.72 \pm 0.02) \times 10^{22}$ cm $^{-2}$).

3.3.1. Pulse Phase Spectroscopy with the $3BB$ model

In the following we present the results from two representative cases: the September 2003 and September 2004 observations. The PPS analysis of the BB components after the latter pointing was hampered by poor statistics. All parameters were left free to vary except for kT_{cold} , R_{cold} and N_{H} that were frozen at the values reported in Table 4. We found that the temperature of the medium and hot BB s were nearly constant through the whole pulse cycle, whereas the normalization/emitting–area were clearly variable (see Figure 6). In order to better study these variations, we fixed the BB temperatures at their phase–averaged values, leaving only the normalizations (N) of the spectra free to vary³. These were then converted into the radii of the BB components ($R_{\text{BB}} = \sqrt{N} \times D_{10}$, assuming a source distance of 3.5 kpc). Figures 7, 8 and Table 5 show our results. In particular, in September 2003 the ratio $\Delta = R_{\text{max}}/R_{\text{min}}$ for each component was $\Delta R_{\text{hot}} = 1.8 \pm 0.1$ and $\Delta R_{\text{med}} = 1.5 \pm 0.2$, while in September 2004 $\Delta R_{\text{hot}} = 1.3 \pm 0.1$, $\Delta R_{\text{med}} = 1.2 \pm 0.1$. In both cases, the modulation of the radii (R) with phase shows only one peak for pulse cycle. Moreover, they appear to be phase–aligned with each other and with the peak of the total pulse profile. This suggests that the two BB regions must be relatively close to each other and likely connected, otherwise a phase lag/shift would naturally be expected. The R –variation amplitude as a function of phase is more pronounced at higher energies, in agreement with the timing properties of this pulsar, where the pulsed fraction is larger at higher energies.

3.3.2. Pulse Phase Spectroscopy of the ~ 1.1 keV edge

A similar analysis was carried out for the narrow spectral feature detected in the spectra from the March 2005 observation onwards. Given the relatively small number of photons, we reduced the number of phase intervals to five and kept the spectral parameters of the coldest BB fixed ($3BB$ +edge model value). In Figure 9 and Table 6 we report the result for the September 2005 observation, when there was a possible indication that the component evolved with phase. Although the value of τ_{max} is compat-

Table 5. R_{med} and R_{hot} as a function of pulse phase for the September 2003 and September 2004 observations. Temperatures are kept fixed at the value listed in Table 4. 1σ confidence level uncertainties are given. The corresponding χ^2_{red} are 0.92 (for 852 d.o.f.) and 1.01 (1132 d.o.f.) for September 2003 and 2004, respectively.

Phase bin	Sept 03 R_{med} km	Sept 03 R_{hot} km	Sep 04 R_{med} km	Sep 04 R_{hot} km
0.0–0.1	5.1 ± 0.4	1.19 ± 0.03	4.3 ± 0.1	0.750 ± 0.001
0.1–0.2	5.3 ± 0.4	1.18 ± 0.05	4.6 ± 0.1	0.82 ± 0.02
0.2–0.3	5.8 ± 0.5	1.31 ± 0.05	4.6 ± 0.1	0.88 ± 0.01
0.3–0.4	6.3 ± 0.5	1.60 ± 0.06	4.6 ± 0.1	0.97 ± 0.01
0.4–0.5	7.2 ± 0.5	1.92 ± 0.06	4.7 ± 0.1	0.91 ± 0.01
0.5–0.6	7.8 ± 0.4	2.10 ± 0.06	4.6 ± 0.1	0.91 ± 0.01
0.6–0.7	7.2 ± 0.4	2.10 ± 0.05	4.5 ± 0.1	0.81 ± 0.02
0.7–0.8	6.7 ± 0.4	1.89 ± 0.04	4.3 ± 0.1	0.83 ± 0.02
0.8–0.9	6.3 ± 0.4	1.55 ± 0.03	4.1 ± 0.1	0.65 ± 0.02
0.9–1.0	6.0 ± 0.3	1.27 ± 0.04	4.2 ± 0.1	0.77 ± 0.02

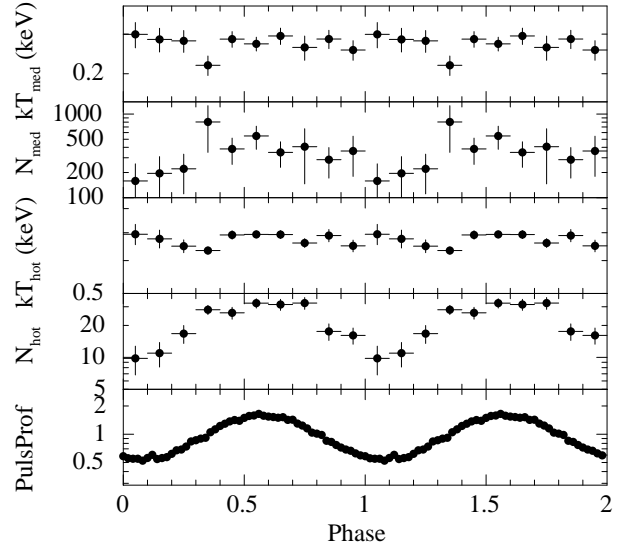


Fig. 6. Phase evolution of BB_{med} and BB_{hot} for the September 2003 observation. The two temperatures remained constant to within the uncertainty, while the normalization changed; the ratio Δ between N_{max} and N_{min} is $\Delta N_{\text{hot,med}} = N_{\text{max}}/N_{\text{min}} \sim 3.3$ and both peak at the same pulse phase (~ 0.55).

ible with being constant ($\chi^2 = 6.57$ with 4 d.o.f.), we note that it varies from a minimum of 0.13 ± 0.06 to a maximum of 0.31 ± 0.07 in a smooth way, which we tried to model with a simple sinusoidal function. An F–Test for the addition of the sinusoid gave just a marginal detection ($\sim 2.4\sigma$), hence no claim can be made about its actual presence. However this possible modulation is worth further investigation with deeper observations.

4. Discussion

The spectral and temporal information obtained from the nine *XMM–Newton* observations of the Transient Anomalous X–ray Pulsar XTE J1810–197 collected in

³ In the “blackbodyrad” model the normalization is $N = R_{\text{km}}^2/D_{10}^2$, with $D_{10} = 0.35$ the distance to the source in units of 10 kpc.

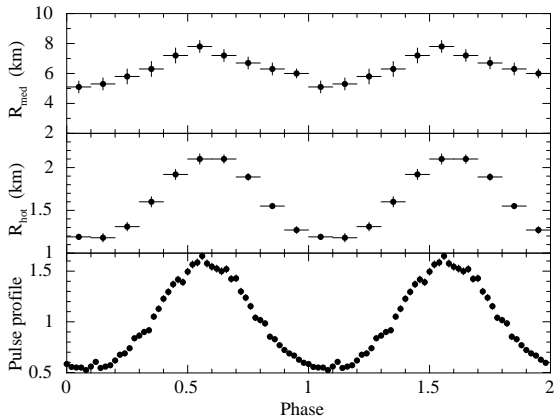


Fig. 7. R_{med} and R_{hot} as a function of rotation phase for the September 2003 observation. The temperatures kT_{med} and kT_{hot} are held fixed at the phase average value listed in Table 4, while the normalization constant (which is related to the radius) is left free to vary.

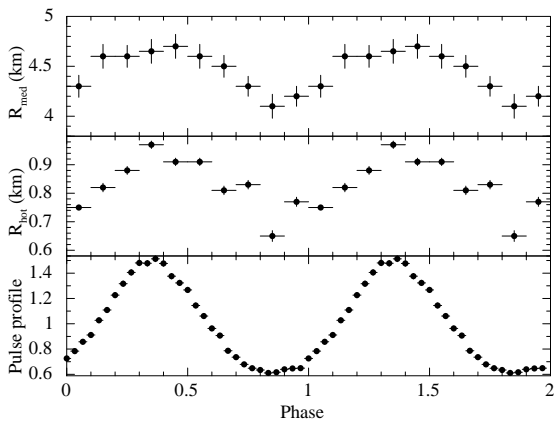


Fig. 8. R_{med} and R_{hot} as a function of rotation phase for the September 2004 observation. The temperatures kT_{med} and kT_{hot} are held fixed at the phase-averaged value listed in Table 4, while the normalization constant (which is related to the radius) is set free to vary.

2003–2007 allowed us to study to an unprecedented level of detail the source behavior during the outburst. As discussed below, our results shed some light on several issues concerning the mechanism powering the emission during the active period. During four years of monitoring, the X-ray flux of XTE J1810–197 continued to decrease following an almost exponential decay. In September 2007 the source nearly reached its quiescent emission level as recorded by *ROSAT* in 1992. In the following we summarize the most relevant findings that we obtained from the *XMM–Newton* dataset.

4.1. The continuum spectral component

We found that the previously proposed *2BB* model for the source spectrum during the outburst fails to account for the time evolution of the hot-temperature

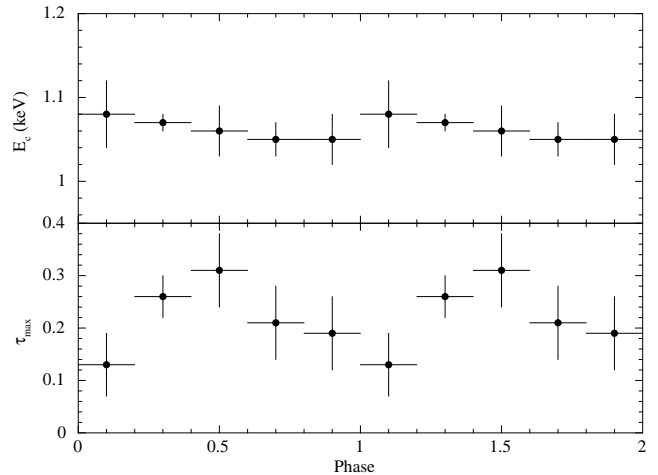


Fig. 9. Evolution of the edge parameters E_c , and τ_{max} with pulse phase for the September 2005 observation (1σ confidence level uncertainties are reported).

Table 6. Evolution of the spectral parameters for the edge component as a function of phase for the September 2005 observation (PN data). 1σ confidence level are reported. The five spectra are fitted together and resulting in a χ^2_{red} of 1.01 (for 406 d.o.f.).

Phase bin	E keV	τ_{max}
0.0–0.2	1.08 ± 0.04	0.13 ± 0.06
0.2–0.4	1.07 ± 0.01	0.26 ± 0.04
0.4–0.6	1.06 ± 0.03	0.31 ± 0.07
0.6–0.8	1.05 ± 0.02	0.21 ± 0.07
0.8–1.0	1.05 ± 0.03	0.13 ± 0.07

spectral components and for the PF flattening (see §3.2.1). Similar concerns have been expressed already by Israel et al (2007b) and Perna & Gotthelf (2008), but see e.g. Güver et al. (2007) for a different interpretation. For these reasons we included a third softer thermal component which, as we have shown in the previous sections, much improves the spectral fits and also removes the inconsistency that appears in the *2BB* model when the evolution of the PF is considered. The temperature and radius of this additional *BB* turn out to be the same as those inferred from the XTE J1810–197 *ROSAT* spectra serendipitously collected since 1992, when the source was in quiescence.

The additional *BB* component is compatible with being emitted from the whole NS surface, and appears to be unaffected by the outburst. Therefore, its nearly constant flux can be taken as representative for the minimum level of emission from the source. It also provides the key to understanding the previously unexplained PF flattening. We emphasize that the *3BB* model discussed here should be regarded as a crude, albeit convenient, description of a scenario in which other effects may come

into play (see below). Nevertheless, it has the advantage of being independent of the, often poorly known, details of the atmosphere/magnetosphere of the neutron star. As such, it provides a first estimate of some key physical parameters, like the size and temperatures of the emitting region(s), without relying on any assumptions about the field strength or geometry. Intriguingly, our analysis reveals that only the size of the hot/warm regions varied during the outburst, showing an almost steady decrease, while the temperatures remained nearly constant.

Although present data do not allow to tightly constrain the shape and relative position of the hot and medium temperature regions on the star, a simple model can be used to gain some insight on the geometry of the source. We assume that emission comes from two concentric zones: an inner, hot cap, and an outer, warm corona, outside of which is the colder surface of the star at $T_{\text{cold}} = 0.160 \text{ keV}^4$, a picture very similar to that adopted by Israel et al. (2007b). For a NS of $1.4 M_{\odot}$ and typical NS radii, we computed the PFs after applying the proper relativistic corrections. Since the angular (semi)aperture of the two zones follows from the values of the blackbody radii, and their temperatures are just kT_{hot} and kT_{med} , the only free parameter is the angle between the diameter through the cap center and the rotation axis, i.e. the cap’s colatitude. The observed spectrum and the lightcurves also depend on the angle between the line of sight (LOS) and the rotation axis. Without performing any formal fit, we simply tried various combinations of these angles, and we found that there is reasonable agreement between PF data and model at all epochs for values which are consistent with the range determined by the detailed analysis of Perna & Gotthelf (2008; see also Kramer et al. 2007 for constraints on the pulsar geometry through radio polarimetry). This is not unexpected since the spectrum in the first 4 epochs, which Perna & Gotthelf analyzed, is not much affected by the emission from the coldest part of the star surface.

We note that our analysis based on the *3BB* model suggests that the coldest *BB* component, accounting for the emission from the whole surface, has a low pulsed fraction, $10\% \pm 1\%$. If our model is correct, this prediction can be checked once the source returns to the quiescent state. We also note that this value is similar to that found in X–ray Dim Isolated Neutron Stars (XDINSSs), where it is believed that the (purely) thermal emission comes from the cooling NS surface (e.g. Haberl 2007). Although magnetars as a class are probably far from being passive coolers, this similarity makes a case for our interpretation of the cold *BB* component as the quiescent emission from the NS surface, worth being pursued in future studies.

On the other hand, the narrower pulse profile and larger pulsed fraction at increasing energies seems reminiscent of what was found for other AXPs with *RXTE* and *INTEGRAL* in the energy band above 10 keV. Indeed, the narrowing of the peak is coincident with the

emergence of a hard power–law component extending from 10–20 keV up to 200 keV at least (Kuiper et al. 2004). The origin of this component is most likely magnetospheric. The marginal detection, during the first three *XMM–Newton* pointings, of a possible hard power–law tail extending above 10 keV, corroborates this reasoning. However we could not study in more detail the power–law tail, due to insufficient statistics.

We performed also a preliminary test with a different model, a simple Comptonization model available in *XSPEC (CompTT)*, but this gives a worse fit for the data with respect to the *3BB* model. More advanced RCS models in which the optical depth is provided by currents flowing in a twisted magnetosphere (Lyutikov and Gavril 2006; Fernandez & Thompson 2007; Nobili, Turolla & Zane 2008a, b) appear, on the other hand, promising in explaining the pulse profiles, since the particle density changes with the magnetic colatitude, increasing as one moves from the magnetic pole towards the equator. Such a distribution naturally introduces a pulsed fraction even in the case in which the surface temperature is homogeneous, as recently shown on the basis of Montecarlo simulations by Nobili et al. (2008a) and Pavan et al. (in preparation). A first attempt to systematically apply RCS to all AXPs, including XTE J1810–197 has been reported by Rea et al. (2008). These authors found that the outburst of this source may result from heating of the NS surface, which slowly cools on a timescale of months/years, while the magnetospheric properties show only small variation during the outburst decay.

4.2. The narrow feature at $\sim 1 \text{ keV}$

Within the framework of the magnetar model, a natural interpretation for the absorption–like feature which is significantly detected in the PN and MOS spectra is that it is due to a proton cyclotron line. The observation of such a feature would directly probe the magnetic field strength of the AXP, since the line energy is proportional to the field strength:

$$E_{\text{cyc}} = 0.63(1+z)^{-1} \left(\frac{B}{10^{14} \text{ G}} \right) \text{ keV} \quad (1)$$

where $(1+z)^{-1} = (1 - 2GM/Rc^2)^{\frac{1}{2}} \simeq 0.8$ is the gravitational redshift at the neutron star surface. Here we assumed $M = 1.4M_{\odot}$ and $R = 10 \text{ km}$ for the star mass and radius. Despite a few earlier claims (Ibrahim et al. 2002; Rea et al. 2003), unambiguous evidence of the presence of absorption lines in the spectra of magnetars has not yet been obtained.

If the edge detected in the XTE J1810–197 spectra is a proton cyclotron feature, when taken face value its energy implies $2.1 \times 10^{14} \text{ G} \leq B_{\text{prot}} \leq 2.6 \times 10^{14} \text{ G}$. On the other hand, the assumption of a constant field breaks down if the line originates from a relatively large region on the neutron star surface/magnetosphere. For instance, Zane et al.

⁴ The radii of these regions are taken from table 3.

(2001) estimated that, even for a simple dipolar field, the fact that B changes in both magnitude and direction will produce a broadening of a feature which is emitted by the whole surface (typically by 10%–20%) and a shift of the line centroid toward lower energies by 20%–30% with respect to the prediction based on eq (1).

Similar absorption features are also observed in the spectra of XDINSs (Haberl 2007) and are typically associated with proton cyclotron and/or bound–free, bound–bound transitions in H, H–like and He–like atoms in the presence of relatively high magnetic fields $B \approx 5 \times 10^{13}$ – 10^{14} G (e.g. van Kerkwijk & Kaplan 2007; Ho et al., 2003; Pavlov & Bezchastnov, 2005). At such large field strengths, exotic molecules might also contribute to line formation (Turbiner et al. 2007, Turbiner & Lopez–Vieyra, 2006). For XDINSs, all the above mentioned scenarios provide similar values of B , which turns out to be in agreement with those derived from the spin–down rate (e.g. Kaplan 2008). A similar absorption feature has been discovered in the spectrum of the Rotating Radio Transient (RRAT) detected at X–ray energies, J1819–1458 (McLaughlin et al. 2007). The X–ray spectrum of RRAT J1819–1458 is well fit by an absorbed blackbody with $kT = 0.14$ keV with the addition of an absorption feature at ~ 1 keV, which, when interpreted either as a proton cyclotron line or as an atomic transition, yields a magnetic field of 5×10^{13} G, again in rough agreement with the spin–down measure (McLaughlin et al. 2007). Also in the case of XTE J1810–197, the magnetic field value inferred by using eq. (1) appears to be in very good agreement with that obtained through the spin–down measurement: 2.2×10^{14} G $\leq B_{\text{dip}} \leq 3.1 \times 10^{14}$ G. It is interesting to note that a similar value, $B = (2.72 \pm 0.03) \times 10^{14}$ G was obtained by Güver et al. (2007) based on the September 2003 – March 2006 *XMM–Newton* spectrum of XTE J1810–197. It is worth emphasizing that the spectral model used by Güver et al. (2007), has been specifically developed for passively cooling NS and magnetic field stronger than 5×10^{13} G and is, therefore, rather different from the $3BB$ model adopted here.

A different possibility is that the line is due to the presence of Iron in proximity of the star surface. In particular, L shell electronic transitions of Iron ions XXII, XXIII, XXIV, have energies between 1.05 and 1.17 keV. However this requires that the line absorbing region is permeated by a relatively low magnetic field. Future longer observations, with much higher statistics, might help to better understand the nature of this spectral feature.

4.3. Flux evolution

During approximately four years of *XMM–Newton* monitoring, the X–ray flux of XTE J1810–197 continued to decrease, and is presently $\sim 15\%$ – 20% above the quiescent level (as determined by *ROSAT*). In Figure 10 the evolution of the total X–ray flux in the 0.6–10 keV band is

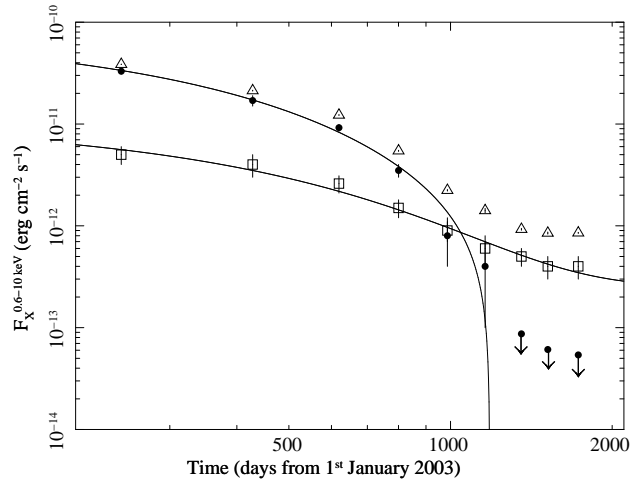


Fig. 10. Evolution of the 0.6 – 10 keV flux (as measured with the EPIC/PN camera on board *XMM–Newton* of XTE J1810–197 as a function of time, for the BB_{med} (squares), the BB_{hot} (circles), and the sum of the $3BB$ s (triangles). The solid line represents the best fit obtained for the BB_{med} and $3BB$ evolution by using a model consisting of an exponential decay plus a constant.

shown (triangles), together with the flux evolution of the two hotter BB s, BB_{med} (squares) and BB_{hot} (circles). Notably, both the BB_{med} and BB_{hot} flux evolutions are well fit by an exponential decay plus a constant ($\chi^2 = 2$ for 5 d.o.f. and $\chi^2 = 5$ for 2 d.o.f., respectively). The characteristic times are $\tau = 370 \pm 40$ days and $\tau = 250 \pm 10$ days for BB_{med} and BB_{hot} , respectively. This might hint towards a common physical process responsible for the decay of the two BB components, though on slightly different timescales. A possible flattening in the BB_{med} flux evolution, as suggested by the latest two/three flux measurements, might imply that this component has already reached its quiescent state (see discussion below).

In order to further test this hypothesis we superimposed the average spectral model, referred to the latest three *XMM–Newton* observations (September 2006 – 2007, where only the BB_{cold} and BB_{med} components are detected), to the average *ROSAT* spectrum obtained by merging the three longest pointings (total effective exposure of ~ 22 ks). This model is compared with the single BB model used so far for the *ROSAT* data. The result of this test is shown in Figure 11. It is evident from the first and second panel that the September 2006 – 2007 *XMM–Newton* model is in agreement with the *ROSAT* data in consideration of the fact that no fit has been performed, suggesting that the source might be already back to its quiescent state since March 2007. If correct, the quiescent state of XTE J1810–197 could be characterized by the presence of two BB s instead of one BB as discussed so far. However, we emphasize that the inclusion of the second BB in the *ROSAT* spectral fit is formally not statistically required. In fact we reanalyzed the *ROSAT* data by using either a single BB or a $2BB$

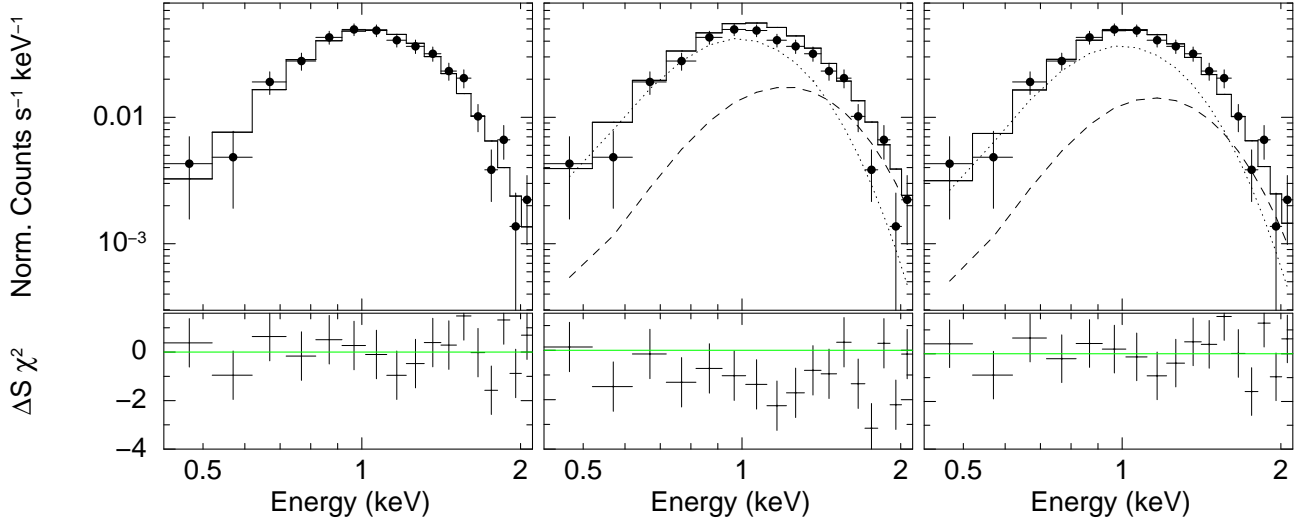


Fig. 11. *ROSAT* PSPC spectrum of the pre-outburst quiescent state of XTE J1810–197 (three PSPC observations were merged together to rely upon a higher S/N), fitted with one *BB* component (left panel), same *ROSAT* spectrum with superimposed the *2BB* model inferred from the latest three *XMM–Newton* observations (since September 2006 the BB_{hot} is not detected; no fit was performed; middle panel), same as before but leaving free to vary the *2BB* model parameters (right panel). The dotted and dash–stepped lines mark the BB_{cold} and BB_{med} components, respectively.

model, and in both cases we obtained a $\chi^2_{\text{red}}=0.9$ (left and right panels of Figure 11). The best fit parameters are: (*BB*) $N_{\text{H}}=(0.63\pm 0.05)\times 10^{22}\text{cm}^{-2}$, $kT=0.19\pm 0.03\text{keV}$ and $R < 11\text{ km}$ ($\chi^2 = 13$ for 14 d.o.f.), (*2BB*) $N_{\text{H}}=(0.75\pm 0.08)\times 10^{22}\text{cm}^{-2}$, $kT_{\text{cold}}=0.16\pm 0.03\text{keV}$ and $R_{\text{cold}}=16\pm 5\text{ km}$, $kT_{\text{med}}=0.26\pm 0.06\text{keV}$ and $R_{\text{med}} < 5\text{ km}$ ($\chi^2 = 11$ for 12 d.o.f.). On the other hand, we note that the *XMM–Newton* model remains slightly above the *ROSAT* data mainly around 1 keV, where the BB_{med} component is maximum. This might suggest that the flux of the latter component is still decaying. Clearly, a deeper and higher–statistics observation of XTE J1810–197 at some later time might solve this issue.

5. Conclusions

In this paper we reported the detailed timing and spectral analysis of a long–term (4 years) *XMM–Newton* monitoring program aimed at unveiling the physical processes responsible for the decaying phases of the XTE J1810–197 outburst. The main results can be summarized as follows:

- We found that a spectral model with three blackbodies is in much better agreement with the data than the previously used model involving two blackbodies. Also, the *3BB* model solves several ambiguities in the spectral evolution that were present in the *2BB* model.
- The best spectral fit at the different epochs is obtained for three blackbodies plus an edge. The best fit spectral parameters determined with this model are: $kT_{\text{cold}} \sim 0.15\text{ keV}$ and $R_{\text{cold}} \sim 15\text{ km}$. The latter feature is required starting from the March 2005 observation, where residuals with respect to the simple *3BB* model are clearly recognized. The coldest *BB* compo-

nent temperature and emitting radius remain constant during the whole outburst and are the same as those of the single *BB* component observed by *ROSAT*, which is likely emitted from the whole NS surface. The two hotter and smaller regions (~ 5 and $\sim 1\text{ km}$) evolve in size but, again, at constant temperature. The emitting surface decreases in both cases and these components are, therefore, likely responsible for the enhancement of the observed X–ray flux during the outburst.

Since September 2006 the hottest component, BB_{hot} , is no longer needed in the fit and the *3BB* model evolves into a *2BB* model. At the same epoch, the average pulsed fraction of the 5.54 s modulation levels up suggesting that the greatest part of the pulsed photons were produced in the BB_{hot} component.

- During the first three *XMM–Newton* observations (2003–2004) the spectral fit residuals suggest the presence of an additional component above 7–8 keV, probably a hard tail, possibly similar to the one detected in other AXPs (where it extends up to 200 keV). The limited sensitivity of the EPIC cameras above 10 keV prevented us from performing a detailed analysis of this component.
- By assuming that the feature around 1.1 keV is due to a proton cyclotron resonance, we obtain a surface magnetic field value of $2.1 \times 10^{14}\text{ G} \leq B_{\text{prot}} \leq 2.6 \times 10^{14}\text{ G}$. This estimate is in very good agreement with that obtained from the spin–down measure of $1.6 \times 10^{14}\text{ G} \leq B_{\text{dip}} \leq 2.8 \times 10^{14}\text{ G}$. We can not currently exclude that the absorption feature originates from L–shell transitions of Fe XXII, XXIII and XXIV.
- The analysis of the pulsed fraction time evolution as a function of energy shows an increase with energy,

within individual observations, and a decrease as a function of time, within the same energy interval. Most of the modulation is ascribed to high–energy photons coming from the two hottest BB emitting regions.

- Pulse phase spectroscopy shows that emission from the two hotter BB s peaks at the same phase interval, suggesting that they are emitted by close–by regions (e.g. two concentric zones).
- The observed (0.6–10 keV) flux evolution of the BB_{med} and BB_{hot} is well described by an exponential decay, with characteristic times of $\tau = 370 \pm 40$ days and $\tau = 250 \pm 10$ days, respectively. This suggests that the same physical process is responsible for the decay of the two thermal components, as already noted by Gotthelf & Halpern (2005). While, in a $2BB$ model, the hot component shows similar time decay ($\tau \sim 300$ days), the decay time of the colder one is longer (~ 900 days). This is in agreement with the presence of a colder component, emitted by the whole the star surface.
- A comparison between the latest three *XMM–Newton* pointings and a re–analysis of the *ROSAT* quiescent spectrum reveals that the BB_{med} component might have already reached its quiescent state.

Acknowledgements. This work is partially supported at OAR through Agenzia Spaziale Italiana (ASI), Ministero dell’Istruzione, Università e Ricerca Scientifica e Tecnologica (MIUR – COFIN), and Istituto Nazionale di Astrofisica (INAF) grants. We acknowledge financial contribution from contract ASI–INAF I/023/05/0 and AAE TH–058. Based on observations obtained with *XMM–Newton*, an ESA science mission with instruments and contributions directly funded by ESA Member States and NASA. This research has made use of data obtained through the High Energy Astrophysics Science Archive Research Center Online Service, provided by the NASA/Goddard Space Flight Center. SZ acknowledges support from a STFC (ex–PPARC) AF. DG acknowledges financial support from the French Space Agency (CNES).

References

- Camilo, F., Ransom, S. M., Halpern, J. P., Reynolds, J., Helfand, D. J., Zimmerman, N., & Sarkissian, J. 2006, *Nature*, 442, 892
- Camilo, F., et al. 2007a, *ApJ*, 669, 561
- Camilo, F., Ransom, S. M., Halpern, J. P., & Reynolds, J. 2007b, *ApJ*, 666, L93
- Camilo, F., et al. 2007a, *ApJ*, 663, 497
- den Herder, J. W., et al. 2001, *A&A*, 365, L7
- Dall’Osso S. et al. 2003, *ApJ*, 599, 485
- Duncan, R. C., & Thompson, C. 1992, *ApJ*, 392, L9
- Fernández, R., & Thompson, C. 2007, *ApJ*, 660, 615
- Gavriil, F. P., Kaspi, V. M., & Woods, P. M. 2004, *ApJ*, 607, 959
- Gelfand, J. D., & Gaensler, B. M. 2007, *ApJ*, 667, 1111
- Gotthelf, E. V., Halpern, J. P., Buxton, M., & Bailyn, C. 2004, *ApJ*, 605, 368
- Gotthelf, E. V., & Halpern, J. P. 2005, *ApJ*, 632, 1075
- Gotthelf, E. V., & Halpern, J. P. 2007, *Ap&SS*, 308, 79
- Götz, D., Mereghetti, S., Tiengo, A., & Esposito, P. 2006, *A&A*, 449, L31
- Güver, T., Özel, F., Göğüş, E., & Kouveliotou, C. 2007, *ApJ*, 667, L73
- Haberl, F. 2007, *ApSS*, 308, 181
- Halpern, J. P., Gotthelf, E. V., Becker, R. H., Helfand, D. J., & White, R. L. 2005, *ApJ*, 632, L29
- Halpern, J. P., Gotthelf, E. V., Reynolds, J., Ransom, S. M., & Camilo, F. 2008, *ApJ*, 676, 1178
- Helfand, D. J., Chatterjee, S., Briskin, W. F., Camilo, F., Reynolds, J., van Kerkwijk, M. H., Halpern, J. P., & Ransom, S. M. 2007, *ApJ*, 662, 1198
- Ho, W. C. G., Lai, D., Potekhin, A. Y., & Chabrier, G. 2003, *ApJ*, 599, 1293
- Ibrahim, A. I., et al. 2002, *ApJ*, 574, L51
- Ibrahim, A. I., et al. 2004, *ApJ*, 609, L21
- Israel, G. L., et al. 2004, *ApJ*, 603, L97
- Israel, G., et al. 2005, *A&A*, 438, L1
- Israel, G. L., Campana, S., Dall’Osso, S., Muno, M. P., Cummings, J., Perna, R., & Stella, L. 2007a, *ApJ*, 664, 448
- Israel, G. L., Bernardini, F., Burgay, M., Rea, N., Possenti, A., Dall’Osso, S. and Stella, L., 2007b, arXiv:0711.04821v1 proceeding.
- Jansen, F., et al. 2001, *A&A*, 365, L1
- Kaplan, D. 2008, in 40 YEARS OF PULSARS: Millisecond Pulsars, Magnetars and More. AIP Conference Proceedings, Volume 983, pp. 331–339
- Kaplan, D.L., Van Kerkwijk, M.H. 2005a, *ApJ*, 628, L45
- Kaspi, V., *Isolated Neutron Stars: From the Interior to the Surface*, *Astrophysics & Space Science*, Springer, Vol. 308, Issue 1–4, pp. 1–11, astro–ph/06103040 (2007)
- Kramer, M., Stappers, B. W., Jessner, A., Lyne, A. G., & Jordan, C. A. 2007, *MNRAS*, 377, 107
- Kuiper, L., Hermsen, W., & Mendez, M. 2004, *ApJ*, 613, 1173
- Kuiper, L., Hermsen, W., den Hartog, P. R., & Collmar, W. 2006, *ApJ*, 645, 556
- Lyutikov, M., & Gavriil, F. P. 2006, *MNRAS*, 368, 690
- Mason, K. O., et al. 2001, *A&A*, 365, L36
- McLaughlin, M., et al. 2007, *ApJ*, 670, 1307
- Muno, M. P., et al. 2006b, *ApJ*, 636, L41
- Muno, M. P., Gaensler, B. M., Clark, J. S., de Grijs, R., Pooley, D., Stevens, I. R., & Portegies Zwart, S. F. 2007, *MNRAS*, 378, L44
- Nobili, L., Turolla, R., & Zane, S. 2008a, *MNRAS*, 386, 1527
- Nobili, L., Turolla, R., & Zane, S. 2008b, *MNRAS*, 389, 989
- Pavlov, G.G., Bezchastnov, V.G., 2005, *ApJ*, 635, L61, 2005
- Perna, R., & Gotthelf, E. V. 2008, *ApJ*, 681, 522
- Rea, N., et al. 2003, *ApJ*, 586, L65
- Rea, N., et al. 2004, *A&A*, 425, L5
- Rea, N., et al. 2005, *MNRAS*, 361, 710
- Rea, N. et al., 2007, *Ap&SS* 308, 505

- Rea, N., Zane, S., Turolla, R., Lyutikov, M., Götz, D. 2008, *ApJ*, 686, 1245
- Schreier, E., Levinson, R., Gursky, H., Kellogg, E., Tananbaum, H., & Giacconi, R. 1972, *ApJ*, 172, L79
- Skinner, S. L., Perna, R., & Zhekov, S. A. 2006, *ApJ*, 653, 587
- Strüder, L., et al. 2001, *A&A*, 365, L18
- Testa, V., et al. 2008, *A&A*, 482, 607
- Titarchuk, L. 1994, *ApJ*, 434, 570
- Thompson, C., & Duncan, R. C. 1995, *MNRAS*, 275, 255
- Turbiner, A.V. et al. 2007, *ApSS*, 308, 267
- Turbiner, A.V., Lopez–Vieyra, J.C. 2006, *Phys. Rep.*, 424, 309
- Turner, M. J. L., et al. 2001, *A&A*, 365, L27
- van Kerkwijk, M. H., & Kaplan, D. L. 2007, *Ap&SS*, 308, 191
- Woods, P. M., Kouveliotou, C., Göğüş, E., Finger, M. H., Swank, J., Markwardt, C. B., Hurley, K., & van der Klis, M. 2002, *ApJ*, 576, 381
- Woods, P. M., et al. 2004, *ApJ*, 605, 378
- Woods, P. M., et al. 2005, *ApJ*, 629, 985
- Woods, P. M., & Thompson, C. 2006, *Compact stellar X–ray sources*, 547
- Zane, S., Turolla, R., Stella, L., & Treves, A. 2001, *ApJ*, 560, 384